Journal of Photochemistry and Photobiology A: Chemistry 225 (2011) 72–80

Contents lists available at SciVerse ScienceDirect

Journal of Photochemistry and Photobiology A: Chemistry

journal homepage: www.elsevier.com/locate/jphotochem

Comparative kinetic model of fluorescence enhancement in selective binding of monochlorobimane to glutathione

Maria Hepel*, Magdalena Stobiecka

Department of Chemistry, State University of New York at Potsdam, Potsdam, NY 13676, USA

ARTICLE INFO

Article history:
Received 15 May 2011
Accepted 27 September 2011
Available online 4 October 2011

Keywords:
Glutathione-monochlorobimane binding
Glutathione Raman spectrum
Binding kinetics
Glutathione fluorimetry
Isothermal calorimetry

ABSTRACT

The highly specific binding of fluorescent label monochlorobimane (MCB) to thiols has been investigated using a tripeptide thiol, glutathione (GSH), a biomolecule protecting cells against oxidative stress and damaging radicals. Due to the reported uneven distribution of MCB in living cells and compartmentalization of GSH in cells, we have explored binding of MCB to GSH in a higher concentration range than normally applied in fluorimetric analysis. Since at higher concentrations, a concentration quenching may interfere with the analysis and because MCB binding to GSH is controlled by kinetics, a special comparative kinetic model of the binding reaction has been developed and utilized in fluorimetric determinations of GSH and in an independent non-optical isothermal reaction-heat measurement. The rate constants: $k_1 = 0.274 \pm 0.012$ and $0.315 \pm 0.004\,s^{-1}\,M^{-1}$, have been obtained from fluorescence and microcalorimetric methods, respectively. The molar enthalpy of binding, $\Delta H = -48.46 \pm 0.61$ kJ/mol, has been determined. The low value of k_1 obtained from fluorimetric measurements precludes concentration quenching for MCB concentrations up to 330 μM and GSH concentrations up to 5 mM. The DFT quantum mechanical calculations have been performed to elucidate changes in vibrational characteristics of bimane fused rings upon GSH binding. The predicted relaxing of rings vibrational modes has been confirmed in Raman scattering spectra and is consistent with the increased fluorescence emission of the adduct. Plausible elucidation of the mechanism of this process is discussed.

Published by Elsevier B.V.

1. Introduction

Fluorescent labeling of cells and their constituents has been widely applied in cell biology and medicine [1,2] enabling studies of key aspects of life processes, such as the signaling pathways, and also studies of the disease, tumor growth, chemotherapy, and others. Furthermore, a direct analysis of proteins, nucleic acids, enzymes and small transmitter or regulatory biomolecules in living cells has become possible [3] owing to fluorescent labeling and high sensitivity of the fluorescence measuring technique. In this work, we have investigated kinetic aspects of selective binding of a fluorescent dye monochlorobimane (MCB) to glutathione (GSH) in view of analytical applications of this reaction to studies of the superficial role that GSH plays in redox maintaining [4] and detoxifying routines in eukaryotic organisms [4–6].

The uneven distribution of MCB in GSH analysis in cells, reported by Briviba et al. [7] and Soderdahl et al. [8], puts into question the usefulness of MCB application in living cells. In this work, we have explored the possibility of increasing the concentration of MCB to higher levels than normally used in fluorimetric analysis and possibly saturate the MCB absorption on nuclei. The problem is that at higher concentrations of MCB and analyte, a concentration quenching may interfere with the analysis. Therefore, to make a reliable assessment of the contribution of this interference, we have performed a comparative kinetic measurement of MCB binding to GSH using a non-optical method, isothermal microcalorimetry (ITC) in which the reaction progress is determined by measuring the reaction heat.

The mono(haloalkyl)bimanes react selectively with thiols to form fluorescent substitution products [1,9]. The syntheses and optical properties of many bimane derivatives have been extensively studied by Kosower and coworkers [9]. The MCB binding to GSH, a tripeptide thiol (γ-glutamyl-cysteinyl-glycine), has been applied widely to monitor the cell signaling pathways and disease development in which GSH level is affected. The rate of binding to MCB, to form a GSH–MCB adduct (GSB), is kinetically controlled. Usually, an enzyme, glutathione S-transferase (GST), is utilized to speed-up the reaction and assist in transferring GSH across the cell membranes, e.g. from the red blood cells (RBC) to the medium, enabling analytical determinations of GSH without disintegrating cell membranes. However, the kinetic enhancement differs considerably between different GST isozymes [10]. The conjugation of MCB with GSH has been widely applied to quantify GSH, map its

* Corresponding author. Tel.: +1 315 267 2267, fax: +1 315 267 3170.
E-mail address: hepelmr@potsdam.edu (M. Hepel).
URL: http://www2.potsdam.edu/hepelmr (M. Hepel).

1010-6030/$ – see front matter. Published by Elsevier B.V.
doi:10.1016/j.jphotochem.2011.09.028

distribution in cells and tissues, and follow various disease development. For instance, in tumor cells, it has been investigated to discern tumor and normal cells [11] and to elucidate mechanisms of tumor cell resistance to chemotherapeutic drugs (adriamycine and 4-hydroperoxycyclophosphamid) [11], developed in some cell lines. The rate of reaction of MCB with GSH measured in human MCF-7 adenocarcinoma cells have shown that cancer cells exhibit significantly higher GSH concentration than normal cells and also show a rapid efflux of the conjugate with up to 85% of conjugate exported within 60 min after delivery. The GSH–bimane adduct has been utilized to determine the GSH level in body fluids and different tissues. For instance, considerable differences in GSH levels in the ocular tissue between normal and galactosemic guinea-pigs have been found [12]. The kinetics of bimane detoxification by enzymatic conjugation to GSH in plants has been studied by Fricker and Meyer [13]. Among other fluorescent dyes highly specific to GSH are: o-phthalaldehyde [14], 2,3-naphthalenedicarboxaldehyde [15], 7-amino-4-chloromethylcoumarin (CMAC) [16], and mercury orange [17]. Recently, monobromobimane has been proposed for the analysis of whole blood sulfide levels in view of the new discovery of hydrogen sulfide as a signaling molecule [18]. We have developed a very sensitive fluorescent DNA-beacon turn-on probe for GSH [19] based on competitive mercury ligation which enabled determinations of GSH and cysteine with a very low limit of detection (LOD) of 4 nM, in a matrix of amino acids.

The oxidative stress which has been implicated in many diseases and can lead to serious damage to DNA (formation of 8-oxoguanine, lesions, strand breaks) and lipids (oxidation to genotoxic 4-hydroxy-2-nonenal [5]), is counteracted and prevented in healthy cells by the homeostasis of the GSH/GSSG redox couple [6]. In clinical studies on autistic children [4], a depletion in GSH level has been found and the development of this debilitating disease attributed, at least partly, to GSH deficiency. Therefore, screening of the oxidative stress biomarkers (GSH and others) on a wide scale becomes an important issue.

The analytical methods for determination of GSH are based on spectrophotometry [20–22], HPLC [23–25], mass spectrometry [26], voltammetry [27–30], and colorimetric sensors [31–36]. Other techniques include resonance elastic light scattering (RELS) of modified gold nanoparticles [37,38] and their plasmonic spectroscopy [39]. The biorecognition-based sensors, including immunosensors, can also be applied for the analysis of GSH. An extensive review of immunosensors has been published by Skladal et al. [40,41]. The pioneering works in developing immunosensors for GSH have been done by Cliffel and coworkers [42]. They have immobilized the anti-GSH antibody on a protein A layer adsorbed nonspecifically on a gold electrode and monitored the response to GSH-conjugates by recording shifts of the oscillation frequency of a quartz piezoresonator substrate. We have also developed a molecularly templated conductive polymer sensor for GSH and GSH-capped gold nanoparticles [29].

The interactions of GSH with gold surfaces has been found to be very strong due to the formation of thiolate bonds with surface Au atoms [43–45] and has been extensively studied to evaluate ligand exchange and competition with homocysteine, which is an important biomarker of oxidative stress, diabetes, and cardiovascular disease [37,39].

In this work, we have investigated the interactions of GSH with MCB in view of their bioanalytical applications for determination of GSH in cells and body fluids and potential uses in screening blood samples for GSH level in autistic children [4]. Due to the uneven distribution of MCB (with preference to nucleus), we have explored the binding of MCB to GSH for increased concentrations of MCB to a higher level than normally used in fluorimetric analysis and avoided adding GST to simplify the reaction pathway. The interactions of GSH with MCB are irreversible and therefore, the system kinetics has been examined. A kinetic model has been developed for fluorescence analysis and independent measurements of heat flux generated by the binding reaction using isothermal calorimetry (ITC) have been carried out to assess if concentration quenching is interfering or not at higher analyte concentrations in fluorimetric analysis. Molecular modeling has been applied for the assessment of changes in the bimane double-ring vibrational characteristics that lead to the enhanced fluorescence upon GSH binding. Raman scattering spectroscopy has confirmed conclusions from molecular modeling investigations.

2. Materials and methods

2.1. Chemicals

All chemicals used for investigations were of analytical grade purity. Monochlorobimane (MCB; $C_{10}H_{11}ClN_2O_2$; 1,5-diazabicyclo[3.3.0]octadiene-2,8-dione) was obtained from Fluka Chemical Corp. (Milwaukee, WI, U.S.A.) and L-glutathione (GSH; $C_{10}H_{17}N_3O_6S$; γ-L-glutamyl-L-cysteinyl-glycine), minimum 99%, from Sigma–Aldrich Chemical Company (St. Louis, MO, U.S.A.). Sodium phosphate monobasic ($NaH_2PO_4{\cdot}2H_2O$) and dibasic ($Na_2HPO_4{\cdot}7H_2O$), and other chemicals were obtained from Fisher Scientific Company (Pittsburgh, PA, U.S.A.). Solutions were prepared using Millipore (Billerica, MA, U.S.A.) Milli-Q deionized water (conductivity $\sigma = 55$ nS/cm). They were deoxygenated by bubbling with purified argon.

2.2. Apparatus

The fluorescence spectra were recorded using a model LS55 Spectrometer (Perkin Elmer, Waltham, MA, USA) equipped with 20 kW xenon light source operating in 8 μs pulsing mode. Separate monochromators for the incident beam and the detector beam enabled to use monochromatic radiation with wavelengths from 350 nm to 700 nm. The dual detector system consisted of a photomultiplier tube (PMT) and an avalanche photodiode. The UV–vis spectra were recorded using a model Varian Cary 50 Bio spectrophotometer (Agilent Technologies, Santa Clara, CA, U.S.A.) in the range from 200 nm to 800 nm at room temperature. Standard polystyrene cuvettes with a path length of 1 cm were used for UV–vis and fluorimetric measurements. The isothermal calorimetry experiments were performed using a model Nano ITC manufactured by TA Instruments (Lindon, UT, U.S.A.). The Raman spectra were recorded using a Nicolet DXR Raman Microscope (Thermo Fisher Scientific, Waltham, MA, U.S.A.). The samples of GSH with MCB for Raman experiments were prepared from a solution by casting on tin foil-coated glass slides. Powders of MCB and GSH obtained from Sigma Company were used without further treatment and purification. Raman measurements were performed in a closed chamber using stabilized 633 nm He–Ne laser with 8 mW power, focused onto a 0.8 μm diameter spot, and measured in the spectral range of 500–3500 cm^{-1}.

2.3. Procedures

The stock solutions of 1 mM MCB and 10 mM glutathione, both in 20 mM phosphate buffer pH 7.4 containing 10% methanol, were used in experiments (methanol was added due to relatively low solubility of MCB). They were stored at 4 °C at all times. In isothermal calorimetry experiments, the reference cell in the Nano ITC was filled with 20 mM phosphate buffer containing 10% methanol. The MCB solution was loaded into a 360 μL volume of sample cell of the calorimeter and GSH in the same buffer was placed in a 50 μL syringe. The system was allowed to equilibrate and a stable base line was recorded for 300 s before initiating automated

injections. The heat flux was recorded following an injection of 3 μL into the sample cell. The sample cell was closed at 185 μL capacity and stirred at 300 rpm. The temperature of the system was maintained at 25.00 ± 0.01 °C. A control dilution experiment was performed using an identical injection of GSH into a cell containing only buffer. The thermal effects due to the tripeptide dilution have been subtracted from the binding reaction heat data.

Molecular dynamics (MD) simulations and quantum mechanical (QM) calculations of electronic structures for a model MCB, GSH and the adduct GSB were performed using density functional theory (DFT) with B3LYP functional and 6-31G* basis set. The molecular dynamics simulations and quantum mechanical calculations were carried out using procedures embedded in Wavefunction (Irvine, CA, U.S.A.) Spartan 6 software. The electron density ρ_e is expressed in atomic units, au^{-3}, where 1 au = 0.52916 Å and $1\,au^{-3} = 6.7491\,Å^{-3}$. The assignment of vibronic frequencies in experimental Raman spectra has been made on the basis of DFT IR calculations and the published data [46,47].

3. Results and discussion

3.1. Absorbance, Raman, and fluorescence emission spectra for MCB interacting with GSH

The electronic π–π* transitions in conjugate double-bond heterostructure of MCB result in the intense yellow color of the dye solutions. The UV–vis spectra recorded for increasing concentrations of MCB, presented in Fig. 1a, show a major absorbance band at λ_{max} = 395 nm. The absorbance maximum A_{max} increases linearly with C_{MCB} as shown in Fig. 1b ($A_{max} = \varepsilon b C_{MCB}$, with extinction coefficient $\varepsilon = 6.170\,M^{-1}\,cm^{-1}$, path length b = 1 cm; correlation coefficient: R = 0.9989). This, and the absence of satellite absorbance peaks at higher or lower frequency, indicates that there are no dimers or higher H- or J-aggregate formation observed in this case.

The halogenated bimane molecules are known to form GSH–bimane adducts with glutathione [9]. However, the absorbance shifts in MCB spectrum upon addition of GSH are minute and cannot be readily discerned. According to Radkowsky and Kosower [9], a small blue shift of 1.5 nm was observed upon addition of GSH to MCB. The GSH itself does not exhibit any electronic transitions in the visible region of electromagnetic spectrum. It is likely that the separation of GSH moiety from the conjugated π–π* fused-ring system of MCB by one methylene group renders the adduct insensitive to the presence of GSH tail. However, a change in the fluorescence emission intensity, as shown below, is observed and forms the basis for analytical procedures of GSH determination. The GSH binding to MCB results in the pronounced change in the Raman spectrum (Fig. 2), with the complete disappearance of the –SH stretching mode of GSH at 2529 cm^{-1}. This clearly indicates that MCB binds GSH through the sulfur atom, as expected. A significant decrease in relative intensity of both the ring vibrations and the peripheral CH_3/CH_2 vibrations is observed. We have compared the relative changes in vibration intensities of various modes by assuming that the symmetric C=O stretching observed in both MCB and GSB at 1709 cm^{-1} is changed the least by the binding process. This enabled us to calculate the relative changes of vibration intensity for other modes. On the basis of this tentative assumption, we have found that the intensity of symmetric stretching of C–H bonds in terminal CH_3 groups in MCB at 2901 cm^{-1} decreased 1.8 times upon GSH binding and that of bending vibrations (scissoring) at 1362 cm^{-1} decreased 3.2 times upon GSH binding. In the group of ring vibrations, asymmetric C=O stretching at 1597 cm^{-1} decreased 2.2 times, asymmetric C=C stretching at 1571 cm^{-1} decreased 1.4 times, N–N stretching at 1004 cm^{-1} decreased 4.3 times, rings breathing at 719 cm^{-1} decreased 1.2 times and symmetric C–N–C stretching at 615 cm^{-1} decreased 2.1 times. All these changes in vibrational characteristics indicate on a decrease of the double-ring vibrations leading to the diminished radiationless energy losses and the enhancement of fluorescence.

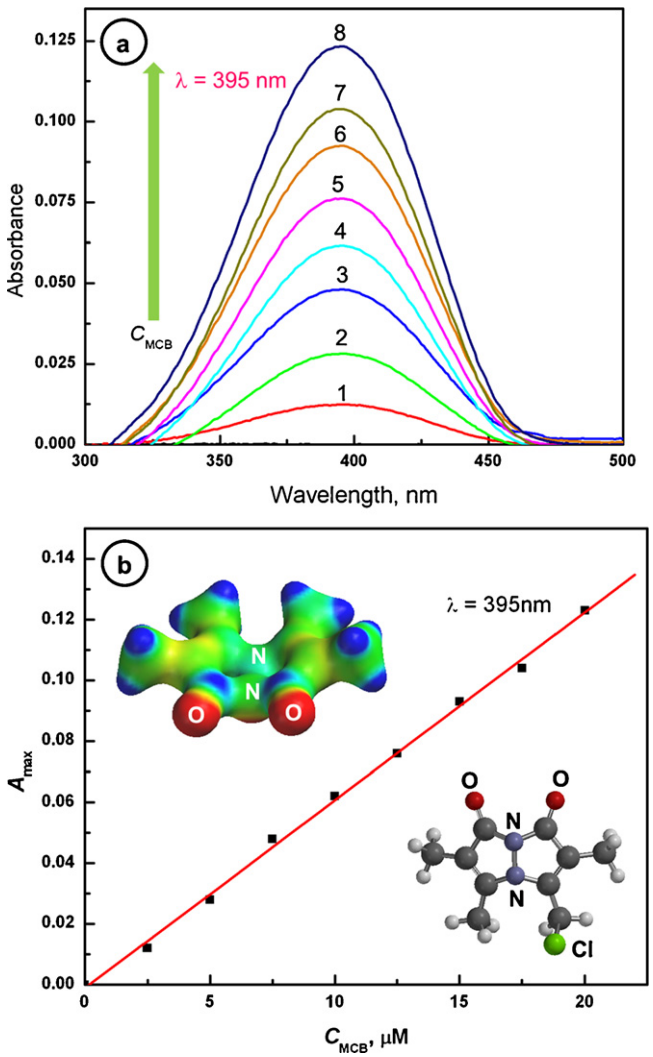

Fig. 1. (a) Absorbance spectra of monochlorobimane, recorded in 20 mM phosphate buffer pH 7.4, for C_{MCB} [μM]: (1) 2.5, (2) 5, (3) 7.5, (4) 10, (5) 12.5, (6) 15, (7) 17.5, (8) 20; (b) dependence of A_{max} vs. C_{MCB}; insets: molecular structure and DFT electron density surface (ρ_e = 0.08 au^{-3}) for MCB.

The fluorescence emission spectra for MCB interacting with GSH have been obtained by setting the excitation wavelength λ_{ex} to MCB absorbance maximum (λ_{ex} = 395 nm). As illustrated in Fig. 3 for a solution of 330 μM MCB + 330 μM GSH in 20 mM phosphate buffer, pH 7.4, a broad emission spectrum with the wavelength of emission maximum λ_{em} = 485 nm, is observed. Fig. 3 shows a clear temporal evolution of fluorescence emission spectra. It appears that the reaction of MCB with GSH is quite slow leading to the increasing emission intensity during the 2-h experiments without reaching a saturation value, indicating that the reaction has not completed.

In Fig. 4, fluorescence emission spectra for MCB–GSH adduct formation recorded after a fixed reaction time t = 50 min are presented. The increase of GSH concentration in solution results in the enhancement of fluorescence emission of MCB. The fluorescence intensity F increases from the background level F_0 due to intrinsic fluorescence of MCB to a saturation level F_{sat} at high C_{GSH} due to the fluorescence of the adduct. The linear response was observed in

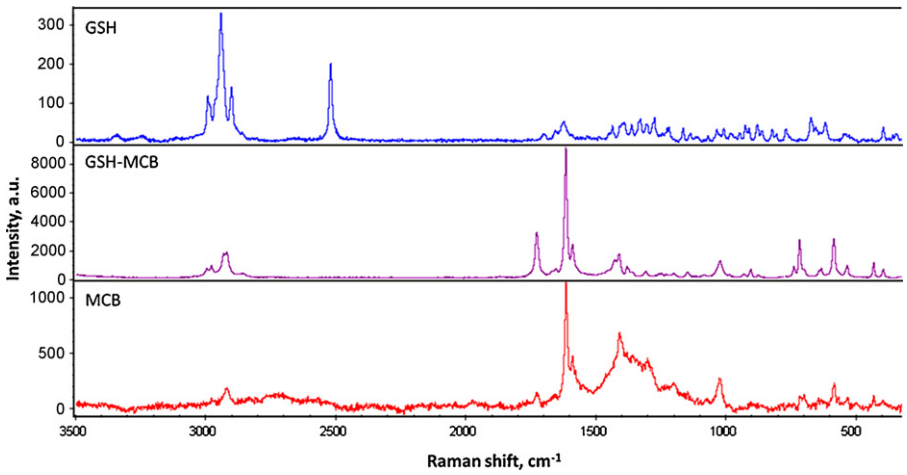

Fig. 2. Raman spectra of (a) GSH alone, (b) adduct GSB, and (c) MCB alone, recorded using a 633 nm He–Ne laser.

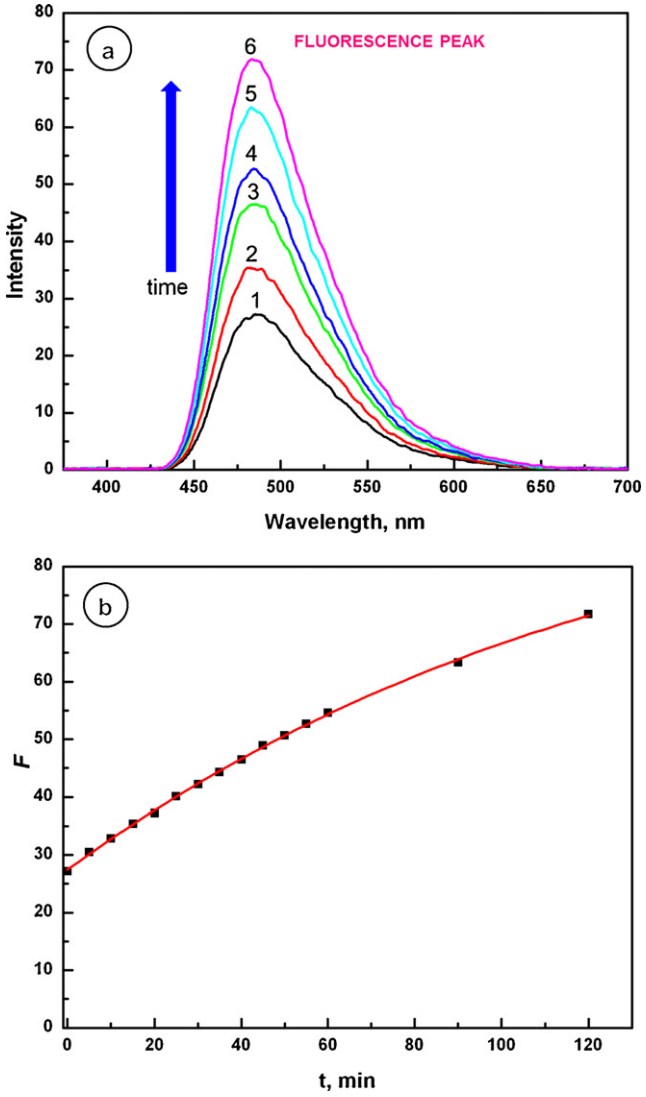

Fig. 3. (a) Temporal evolution of fluorescence emission spectra recorded after mixing monochlorobimane solution with GSH, in 20 mM phosphate buffer pH 7.4; reaction time [min]: (1) 0, (2) 15, (3) 40, (4) 55, (5) 90, (6) 120; λ_{ex} = 395 nm, λ_{em} = 485 nm; C_{MCB} = 330 μM, C_{GSH} = 330 μM (final concentrations); (b) dependence of fluorescence emission intensity maximum *F* vs. time *t*.

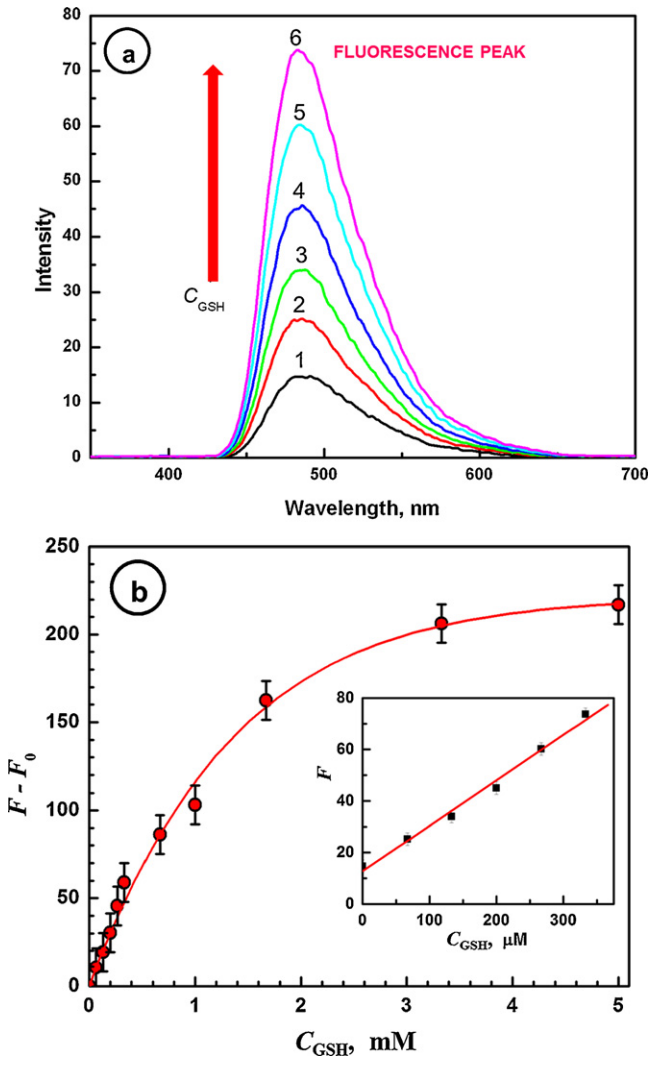

Fig. 4. (a) Fluorescence spectra for 330 μM monochlorobimane solution after adding different concentrations of glutathione, measured after 50 min of the interaction time, C_{GSH} [μM]: (1) 0, (2) 67, (3) 133, (4) 200, (5) 270 (6) 333; (b) dependence of $F–F_0$ vs. C_{GSH}; inset: linear dependence *F* vs. C_{GSH} for lower concentrations of GSH.

the range of C_{GSH} from 0 to 330 μM, with the least-squares fitting given by:

$$F = F_0 + \alpha C_{GSH} \quad (1)$$

where $F_0 = 12.7$, $\alpha = 176.2 \times 10^3\ M^{-1}$ (with C_{GSH} in [M]), correlation coefficient $R = 0.995$. As shown in the next section, α is not equal to the fluorescence coefficient $\varepsilon = (\partial F/\partial C_{0,A})$ defined for reversible systems but depends also on the rate constant and dye concentration.

In the full range of concentrations of GSH studied, the dependence of F vs. C_{GSH} is not linear and can be approximated using a fitting function:

$$F = \frac{F_2 + (F_1 - F_2)}{1 + \exp\{(C_{GSH} - K)/s\}} \quad (2)$$

with the parameters: $F_1 = -250$, $F_2 = 217$, $K = -0.180$ mM, $s = 0.935$ mM; $R = 0.993$. While the shape of the dependence $F = f(C_{GSH})$ resembles that of a binding curve typical of many biorecognition system, this dependence is actually determined solely by the reaction kinetics and not by thermodynamics. The use of fitting equations, such as the one described above, is dictated only by the convenience when any physical model is not available for the system under study. Therefore, in the next section, we present a kinetic model for the interacting system MCB–GSH to be further used in experimental data analysis.

3.2. Kinetic model

An irreversible bimolecular reaction between analyte A (e.g. GSH) and ligand B (e.g. MCB), with the formation of an adduct P and another compound X as the products, can be written as:

$$\underset{C_A}{A} + \underset{C_B}{B} \rightarrow \underset{C_P}{P} + \underset{C_X}{X} \quad (3)$$

where C_A, C_B, C_P, and C_X are the concentrations of reactants. This reaction equation represents the reaction of MCB (denoted here: BCl to show the presence of the Cl-atom substituent in bimane) with GSH written symbolically as:

$$GSH + BCl \rightarrow GSB + HCl \quad (4)$$

The rate v of reaction (3) is given by:

$$v = \frac{\partial C_P}{\partial t} = k_1(C_{0,A} - C_P)(C_{0,B} - C_P) - k_{-1}C_P C_X \quad (5)$$

where k_1 and k_{-1} are the forward and backward rate constants; $C_{0,A}$ and $C_{0,B}$ are the initial concentrations of A and B, respectively. For an irreversible reaction, $k_{-1} \approx 0$, so in further considerations, the second term in Eq. (5) is neglected. In order to analyze kinetic dependences, such as the temporal evolution of fluorescence and calibration plots, this equation has to be integrated. The integration is done in the usual way by separating variables:

$$\int_0^{C_P} \frac{\partial C_P}{(C_{0,A} - C_P)(C_{0,B} - C_P)} = \int_0^t k_1\, \partial t \quad (6)$$

to yield

$$\frac{1}{C_{0,B} - C_{0,A}} \ln\left[\frac{C_{0,B} - C_P}{C_{0,B}} \frac{C_{0,A}}{C_{0,A} - C_P}\right] = k_1 t \quad (7)$$

Hence, the dynamics of the adduct formation can be expressed as:

$$C_P = \frac{C_{0,B}C_{0,A}(1 - \exp\{(C_{0,B} - C_{0,A})k_1 t\})}{C_{0,A} - C_{0,B}\ \exp\{(C_{0,B} - C_{0,A})k_1 t\}} \quad (8)$$

for $C_{0,A} \neq C_{0,B}$. Thus, the fluorescence emission intensity F is given by:

$$F = \varepsilon_B C_B + \varepsilon_P C_P = F_0 + (\varepsilon_P - \varepsilon_B)C_P = F_0 + \varepsilon^* C_P \quad (9)$$

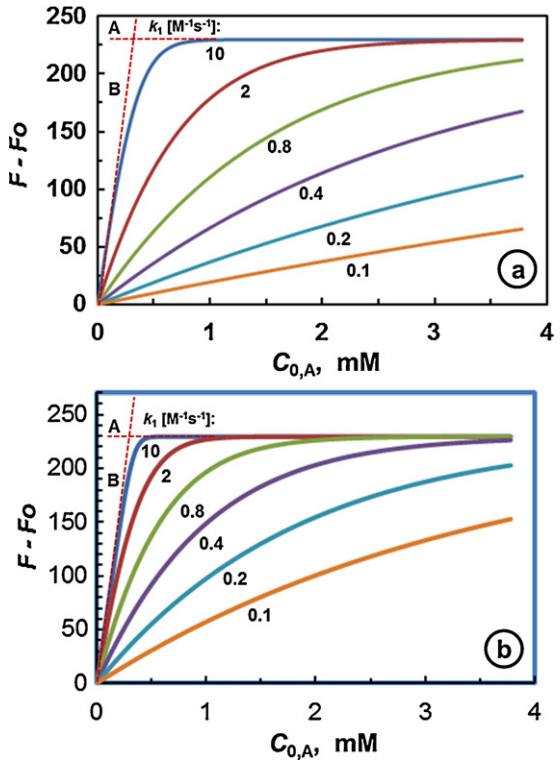

Fig. 5. Dependence of fluorescence emission intensity $F–F_0$ on the initial analyte concentration $C_{0,A}$ for different rate constants k_1 (marked on the graphs) and different reaction time t [s]: (a) 900, (b) 3000, calculated from Eq. (12) for a fluorescent substrate and adduct using the parameters: $\varepsilon_1 = 80\ M^{-1}$, $\varepsilon_2 = 776\ M^{-1}$, $C_{0,B} = 330$ μM; A – saturation level; B – initial calibration slope.

where ε is the fluorescence intensity coefficient, the working parameter ε^* is defined by:

$$\varepsilon* = \varepsilon_P - \varepsilon_B \quad (10)$$

and the fluorescence in the absence of analyte, i.e. for $C_{0,A} = 0$, is given by:

$$F_0 = \varepsilon_B C_{0,B} \quad (11)$$

The dependence of F on time and initial concentrations of the ligand and analyte can be expressed as:

$$F = F_0 + \varepsilon^* C_{0,B}C_{0,A}\frac{1 - \exp\{(C_{0,B} - C_{0,A})k_1 t\}}{C_{0,A} - C_{0,B}\ \exp\{(C_{0,B} - C_{0,A})k_1 t\}} \quad (12)$$

or

$$F = F_0 + (F_{sat} - F_0)x\frac{1 - \exp\{-(1-x)C_{0,B}k_1 t\}}{1 - x\ \exp\{-(1-x)C_{0,B}k_1 t\}} \quad (13)$$

where x is the molar ratio of the analyte to the ligand: $x = C_{0,A}/C_{0,B}$.

Eqs. (12) and (13) provide fitting functions for the experimental data for a kinetically controlled bimolecular interacting system dye–analyte provided that secondary effects, such as the concentration quenching, do not interfere with the analysis. Since this is not known *a priori*, we will call the rate constants determined experimentally, the apparent rate constants. The point at $C_{0,A} = C_{0,B}$ must be excluded due the singularity. A family of analytical calibration curves $F = f(C_{0,A})$ calculated using Eq. (13) for different values of k_1 and for two different incubation times (15 and 50 min) are presented in Fig. 5. It is seen that the initial slope of characteristics changes considerably with k_1 and t.

In the case of concentration quenching, a term proportional to the quencher concentration should be added to Eqs. (12) and (13), for instance for quenching by analyte, a term $-a(C_{0A} - C_P)$, where

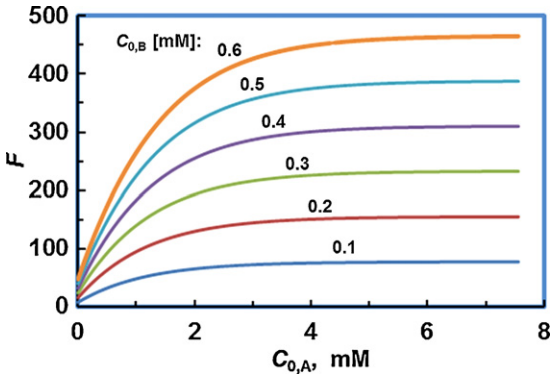

Fig. 6. Dependence of fluorescence emission intensity F on the initial analyte concentration $C_{0,A}$ for different initial dye concentrations $C_{0,B}$ (marked on the graph) from 0.1 to 0.6 mM, calculated from Eq. (12) for a fluorescent substrate and adduct with parameters: $\varepsilon_1 = 80\,M^{-1}$, $\varepsilon_2 = 776\,M^{-1}$, $k_1 = 1\,s^{-1}\,M^{-1}$, and $t = 900\,s$.

a is the quenching coefficient, should be added to the right-hand-side of the equations. If this term is not taken into account, then the value of the apparent rake constant k_1 determined from experimental data would be overestimated. By comparing this values with those obtained by an independent non-fluorimetric method, one can determine if the concentration quenching does take place in the fluorimetric measurements.

The function of Eq. (12) has only two adjustable parameters: ε^* and k_1, which can also be determined graphically from the limiting cases:

(a) For $t \to \infty$, one obtains:

$$\exp\{(C_{0,B} - C_{0,A})k_1 t\} >> 1 \tag{14}$$

and

$$F = F_0 + \varepsilon^* C_{0,A} \tag{15}$$

Therefore, ε^* can be determined from the saturation level of the plots F vs. t, if available.

(b) For short times, $k_1 t \approx 0$, and by linearizing the exponents in (12), one obtains:

$$F \approx F_0 + \varepsilon^* C_{0,A} \frac{C_{0,B} k_1 t}{1 + C_{0,B} k_1 t} \tag{16}$$

and for $C_{0,B} k_1 t \ll 1$

$$F \approx F_0 + \varepsilon^* C_{0,A} C_{0,B} k_1 t \tag{17}$$

Hence, the value of $\varepsilon^* k_1$ can be determined from the slope $(\partial F/\partial t)_{t\to 0} = C_{0,A} C_{0,A} \varepsilon^* k_1$. Therefore, from (a) and (b), both parameters, ε^* and k_1 can be obtained. Otherwise, a nonlinear fitting routine using function (12) for any section of the experimental F–t or F–$C_{0,A}$ dependence can be applied to obtain these parameters. The fitting of experimental data in Fig. 4b, using Eq. (12), provides $k_1 = 0.274 \pm 0.012\,s^{-1}\,M^{-1}$, $\varepsilon^* = 673\,M^{-1}$, with $R = 0.994$. The value of k_1 obtained here compares favorably with k_1 value determined under pseudo-first-order conditions ($k_1 = 0.130\,s^{-1}\,M^{-1}$ [9]).

It is important to realize that the slope $(\partial F/\partial C_{0,A})$ is dependent not only on ε_A and kt but also on $C_{0,B}$ and ε_B, which is unexpected and cannot be deduced *a priori* without derivations presented above. The analytical calibration curves $F = f(C_{0,A})$ calculated using Eq. (13) for different ligand concentrations $C_{0,B}$ are presented in Fig. 6. It is seen that the initial slope of characteristics changes considerably with ligand concentration in agreement with the conclusion drawn above.

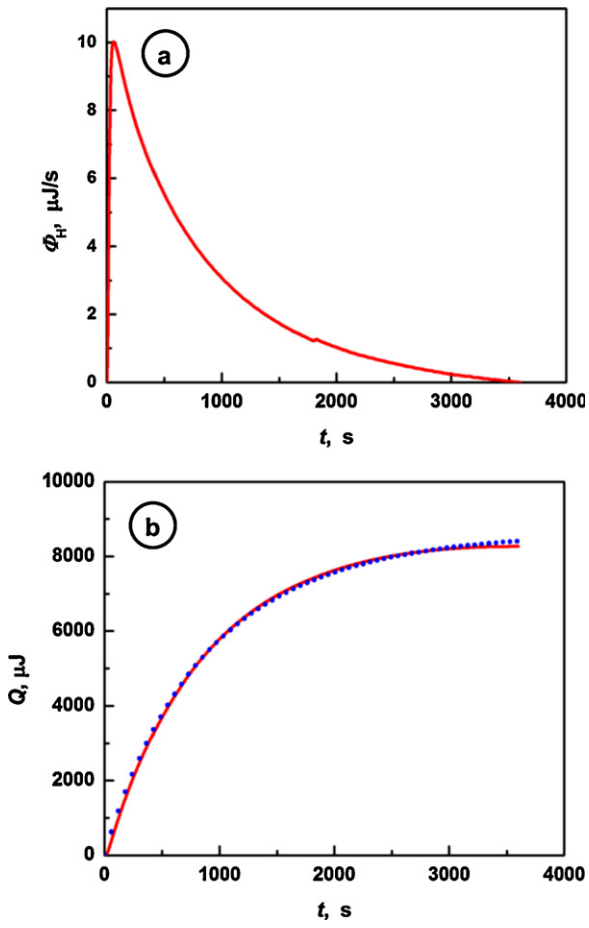

Fig. 7. (a) Heat flux transient, Φ_H vs. t, recorded for an isothermal binding of GSH to MCB upon injection of GSH solution ($C_{0,A} = 0.965$ mM, after dilution) to MCB ($C_{0,B} = 3.95$ mM, after dilution) in a reaction microchamber with volume 185 μL; (b) integrated heat of the binding reaction: line – experimental data; circles – fitting function, Eq. (21).

3.3. Evaluation of MCB–GSH binding kinetics from isothermal reaction-heat generation

Since the secondary effects, such as the concentration quenching, may interfere in fluorimetric analysis of kinetic data, and also because the slow binding of GSH to MCB may proceed through several slow and fast steps which could not be distinguished in fluorescence analysis, another independent method of studying the reaction kinetics was also applied. We have selected the isothermal monitoring of the reaction heat which does not include any optical measurements. Since there is no contribution of effects like concentration quenching in microcalorimetry and since the distribution of the reaction heat among different steps may be different than the distribution of fluorescence emission among these steps, the control experiments carried out using the isothermal calorimetry could potentially provide additional kinetic information about GSH binding to MCB.

The microinjections of a GSH solution to a MCB aliquot were performed using an automated Nano ITC technique. The solution in reaction chamber ($V_{cell} = 185$ μL) was continuously stirred at 300 rpm. A typical ITC transient for binding of GSH to MCB is presented in Fig. 7a. It presents a heat flux decay, $\Phi_H = (dQ/dt) = f(t)$, following the injection of a GSH solution (3 μL, 30 mM) to a 4 mM MCB (both reagents in 20 mM phosphate buffer containing 10% methanol, pH 7.4). After dilution with injected GSH solution, the initial concentration of MCB in reaction chamber was then 3.87 mM

and that of GSH 0.965 mM. The selected recording time (τ = 3600 s) was sufficiently long to enable the reaction completion (Φ_H = 0) and maintaining a flat background. By integrating the heat flux Φ_H over time, a reaction heat transient, $Q = f(t)$, can be obtained:

$$Q(t) = \int_0^{\tau} \Phi_H(t)dt \tag{18}$$

where the reaction heat Q is proportional to the concentration of GSB adduct formed in the reaction (ΔC_P), volume of the ITC cell V_{cell}, and the molar enthalpy of binding reaction ΔH:

$$Q(t) = -\Delta H V_{cell} \Delta C_P \tag{19}$$

In addition, the amount of the product formed in previous tests does not need to be counted since it does not generate any signal (heat flux) and is also not influencing the reaction rate. Hence, in an analogy to equations derived for fluorescence, one obtains:

$$Q(t) = -\Delta H V_{cell} C_{0,B} C_{0,A} \frac{1 - \exp\{(C_{0,B} - C_{0,A})k_1 t\}}{C_{0,A} - C_{0,B}\ \exp\{(C_{0,B} - C_{0,A})k_1 t\}} \tag{20}$$

and

$$Q(t) = Q_{sat} \frac{(1 - \exp\{-(1-x)C_{0,B}k_1 t\})}{(1 - x\ \exp\{-(1-x)C_{0,B}k_1 t\})} \tag{21}$$

where $x = C_{0,A}/C_{0,B}$ and

$$Q_{sat} = -\Delta H V_{cell} C_{0,A} \tag{24}$$

Fitting of the experimental Q–t transients with the function of Eq. (21) has been performed using Levenberg–Marquardt least-squares routine. It is presented in Fig. 7b, where the fitting function is shown (unconventionally) by blue filled circles and the experimental points form a continuous line with 3600 data points. This fitting provides the following parameters: $k_1 = 0.315 \pm 0.001\ s^{-1}\ M^{-1}$, $\Delta H = -48.46 \pm 0.01$ kJ/mol; $R = 0.9988$. The negative value of ΔH indicates that the reaction of GSH with MCB is exothermic. (For 5 transients, std. for k_1 is 0.004 and std. for ΔH is 0.61).

The rate constant determined from ITC transients, $k_1 = 0.315\ s^{-1}\ M^{-1}$, compares favorably with that obtained from fluorescence enhancement measurements ($k_1 = 0.274\ s^{-1}\ M^{-1}$). Therefore, the rate determining step in the GSH binding by MCB is most likely a simple bimolecular reaction. Slightly higher value of k_1 obtained in ITC measurements is probably due to the different way the temperature is maintained (25.00 ± 0.01 °C in ITC vs. 25 ± 1 °C in fluorescence measurements) and higher concentration of reagents necessary to generate enough reaction heat. Since the concentration quenching in fluorescence measurements would have caused an increase of the apparent value of k_1, which is not the case, the important conclusion from ITC results is that the fluorescence data are not obscured by the concentration quenching up to C_{MCB} = 330 μM and up to C_{GSH} = 5 mM.

3.4. Molecular dynamics simulation of GSB conformations

The enhancement of MCB fluorescence upon GSH binding has also been investigated using MD simulations and QM calculations due to unusual circumstances of the enhancement. Usually, when a nonfluorescent chain (such as GSH) is attached to a fused ring structure (such as MCB), a decrease in fluorescence emission is observed. This is often called a "loose-bolt" effect, whereby the added group provides additional vibrational pathways for radiationless energy decay from the excited state of the fused ring structure. However, in the case of GSB, an opposite effect is observed and fluorescence enhancement becomes apparent, as is well known. Although the formation of some third-ring structures has been proposed as the alternative reaction path in the case of dibromobimane [16,48],

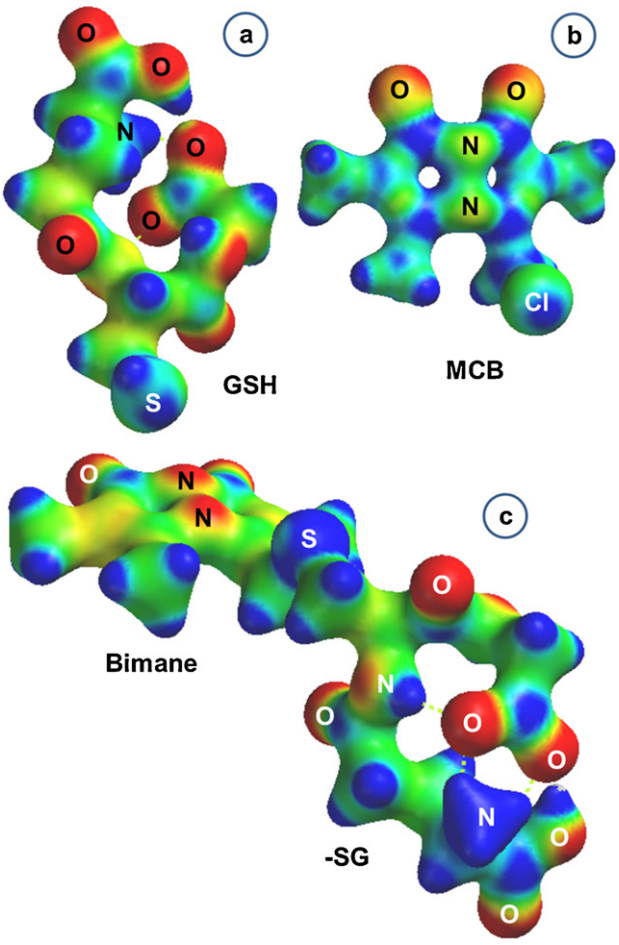

Fig. 8. Electronic structure of (a) GSH in a "tall" conformation, (b) MCB, and (c) the adduct GSB; electron density surfaces were obtained by DFT calculations (ρ_e = 0.1 au^{-3}) and are shown with mapped electrostatic potential (color coded: from more negative – red, to more positive – blue). (For interpretation of the references to color in this figure legend, the reader is referred to the web version of the article.)

these reactions cannot proceed in mono-substituted bimanes. Therefore, we have hypothesized that may be the GSH branches can bend around the bimane molecule and form a ring by binding to the bimane C=O groups. Such binding could be accomplished by hydrogen bonding and would provide an increased stiffness of the bimane fused ring structure. This, in turn, would result in diminished radiationless losses. The question is then whether the GSH branches can reach to the C=O groups on the opposite side of bimane rings and form hydrogen bonds there. The MD simulations show that a selfstanding GSH molecule can form many metastable conformers. This means that there are many local minima in potential energy. When one of such conformers, in a metastable equilibrium, is attached to equilibrated bimane molecule by substituting the chlorine atom in MCB with a –SG moiety, then after the equilibration, a metastable GSB adduct is obtained. It appears that the conformation of -SG branches remains largely unchanged after the equilibration of the adduct and only the substitution region $-CH_2SC-$ is appropriately modified by equilibration routines. In Fig. 8, presented are the MCB and GSH molecules before binding and also the adduct GSB, obtained after equilibration of the adduct. The branches of a GSH molecule, used here in the tall conformation that is held tight with 3 internal hydrogen bonds, are seen to retain this conformation after binding to MCB and equilibration. It is apparent that –SG branches in this conformation do not show any interactions with the bimane –C=O groups. We have tested 4 different GSH conformers: tall, horizontal (wide-spread), and two intermediate structures. The

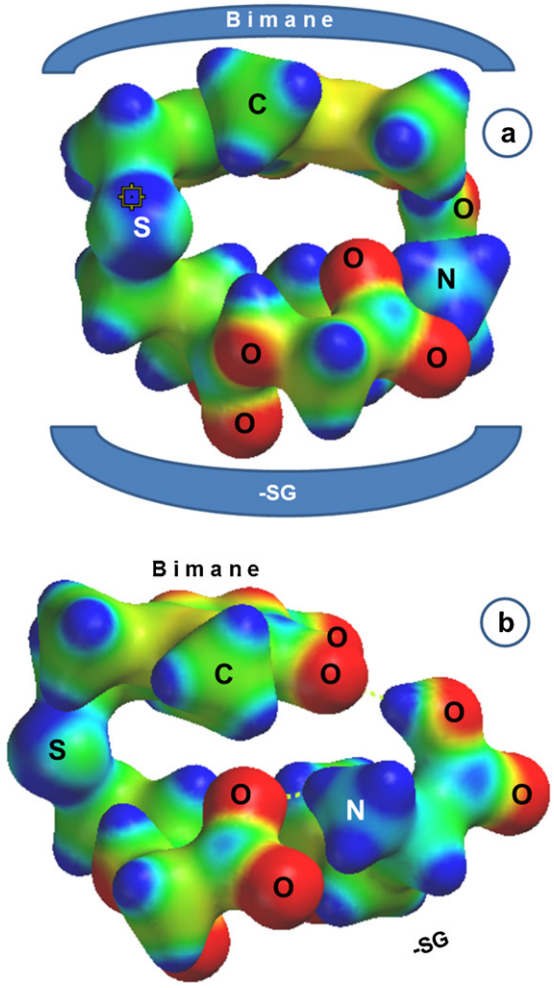

Fig. 9. Electronic structure of GSB conformer showing a hydrogen-bonded loop over the bimane fused rings, stiffening the GSB structure; electron density surface was obtained by DFT calculations ($\rho_e = 0.1$ au^{-3}) and is shown with mapped electrostatic potential (color coded: from more negative – red, to more positive – blue): (a, b) views from different angle. (For interpretation of the references to color in this figure legend, the reader is referred to the web version of the article.)

conformations of –SG branches after binding have remained largely unchanged in all four cases.

By searching through hundreds of GSB conformers, we have found one particular structure, presented in Fig. 9, which shows clearly a loop formed by the glutamyl branch reaching to the –C=O groups on the opposite side of the bimane rings, with a hydrogen bond joining the carboxyl group of the SG arm with –C=O group of bimane rings. This structure may contribute to the fluorescence enhancement exhibited by the GSB adduct. Further studies are on the way to confirm experimentally the viability of this new GSB conformation.

The second effect that may contribute to the fluorescence enhancement is the replacement of the Cl-atom in MCB by an S-atom in GSB. Since the electronegativity of S is lower than that of Cl (2.58 vs. 3.16 [49]), then the inductive electron withdrawal from the conjugated ring system is weaker when S replaces Cl in the GSB adduct. Thus, the ring system is stabilized in the adduct with respect to MCB. This should contribute to the fluorescence enhancement and to the decrease of the intensity of ring vibration modes.

While the effect of diminished inductive electron withdrawal from the bimane rings upon the replacement of Cl-atom with S-atom during the thiol binding is a general feature of thiol binding to MCB, the pronounced fluorescence enhancement observed in GSH binding is likely to be associated with both the change in electron withdrawal effect and possibly also with the formation of a hydrogen-bonded loop. These effects must result in freezing the bimane-rings vibration modes which we have observed in Raman scattering spectra (Fig. 2).

4. Conclusions

The kinetics of GSH binding to MCB has been investigated by following the fluorescence emission transients and the reaction heat flux upon injection of GSH to a solution of MCB. The MD and QM calculations performed to elucidate the mechanisms of changes of the structural and vibrational characteristics of bimane fused rings upon GSH binding have shown that relaxing of vibrational modes of the bimane rings should be observed. We have demonstrated that, indeed, Raman scattering spectra exhibit a diminished intensity of ring vibrations (including C=C symmetric stretching, asymmetric C–N–C stretching, and N–N stretching), as well as other vibrations comprising those in the terminal CH_3 groups. The decrease in the ring vibration mode intensities upon GSH binding to MCB is consistent with the known increased fluorescence emission of the adduct. In addition, the MD simulations suggest that a bimane ring stiffening may also be occurring due to the formation of a hydrogen-bonded loop by the glutamyl arm of SG moiety across the bimane rings to reach one of the C=O groups there. Using a detailed non-enzymatic comparative kinetic model of the GSH–MCB binding reaction, we have demonstrated that no concentration quenching by the analyte is taking place for systems with higher concentrations than normally used in fluorimetric analysis. The isothermal microcalorimetry measurements have provided the basis for this assessment and enabled the extended range treatment in analytical determinations of GSH.

Acknowledgement

This work was supported by the U.S. DoD grant no. AS073218 and NSF grant no. CCLI-0941364.

References

[1] D. Kamencic, A. Lyon, P.G. Paterson, B.H.J. Juurlink, Monochlorobimane fluorimetric method to measure tissue glutathione, Anal. Biochem. 286 (2000) 35–37.
[2] J.R. Lakowicz, Principles of Fluorescence Spectroscopy, Springer, New York, 2006.
[3] W.L. Tseng, K.H. Lee, H.T. Chang, Using Nile Red-adsorbed gold nanoparticles to locate glutathione within erythrocytes, Langmuir 21 (2005) 10676–10683.
[4] S.J. James, S. Melnyk, S. Jernigan, M.A. Cleves, C.H. Halsted, D.J. Wong, P. Cutler, M. Boris, K. Bock, J.J. Bradstreet, S.B. Baker, D.W. Gaylor, Metabolic endophenotype and related genotypes are associated with oxidative stress in children with autism, Am. J. Med. Genet. 141B (94) (2006) 947–956.
[5] R. Kohen, A. Nyska, Oxidation of biological systems: oxidative stress phenomena antioxidants, redox reactions, and methods for their quantification, Toxicol. Pathol. 30 (2002) 620–650.
[6] M. Noble, M. Mayer-Proschel, C. Proschel, Redox regulation of precursor cell function: insights and paradoxes, Antioxid. Redox Signal. 5 (2005) 1456–1467.
[7] K. Briviba, G. Fraser, H. Sies, B. Ketterer, Distribution of the monochlorobimane–glutathione conjugate between nucleus and cytosol in isolated hepatocytes, Biochem. J. 294 (1993) 631–633.
[8] T. Soderdahl, M. Enoksson, M. Lundberg, A. Holmgren, O.P. Ottersen, S. Orrenius, G. Bolcsfoldi, I.A. Cotgreave, Visualization of the compartmentalization of glutathione and protein–glutathione mixed disulphides in cultured cells, FASEB J. 17 (2003) 124–126.
[9] A.E. Radkowsky, E.M. Kosower, Bimanes. 17. (Haloalkyl)-1,5-diazabicyclo[3.3.0]octadienediones (Halo-9,10-dioxabimanes): reactivity toward the tripeptide thiol glutathione, J. Am. Chem. Soc. 108 (1986) 4527–4531.
[10] J.A. Cook, S.N. Iype, J.B. Mitchell, Differential specificity of monochlorobimane for isozymes of human and rodent glutathione S-transferases, Cancer Res. 51 (1991) 1606–1612.

[11] K.K. Millis, S.A. Lesko, M.P. Gamcsik, Formation intracellular distribution and efflux of glutathione–bimane conjugates in drug-sensitive and -resistant MCF-7 cells, Cancer Chemother. Pharmacol. 40 (1997) 101–111.
[12] R. Kannan, D. Tang, J.B. Mackic, B.V. Zlokovic, J.C. Fernandez-Checa, A simple technique to determine glutathione (GSH) levels and synthesis in ocular tissues as GSH–bimane adduct: application to normal and galactosemic guinea-pigs, Exp. Eye Res. 56 (1993) 45–50.
[13] M.D. Fricker, A.J. Meyer, Confocal imaging of metabolism in vivo: pitfalls and possibilities, J. Exp. Bot. 52 (2001) 631–640.
[14] R.N. Puri, R. Roskoski, Reaction of low molecular weight aminothiols with o-phthalaldehyde, Anal. Biochem. 173 (1988) 26–32.
[15] O. Orwar, H.A. Fishman, N.E. Ziv, R.H. Scheller, R.N. Zare, Use of 2,3-naphthalenedicarboxaldehyde derivatization for single-cell analysis of glutathione by capillary electrophoresis and histochemical localization by fluorescence microscopy, Anal. Chem. 67 (1995) 4261–4268.
[16] J. Sebastia, R. Cristofol, M. Martin, E. Rodriguez-Farre, C. Sanfeliu, Evaluation of fluorescent dyes for measuring intracellular glutathione content in primary cultures of human neurons and neuroblastoma SH-SY5Y, Cytometry 51 (2003) 16–25.
[17] R.K. Pierce, A. Owen, S. Daniel, P. Jenner, C.D. Marsden, GSH mercury orange fluorimetry, J. Neural Transm. 104 (1997) 661–677.
[18] A. Bengtsson, J. Johnson, P. Hill, J. Muligan, D. Leviten, M. Insko, et al., Use of mono-bromo-bimane to derivatize sulfide levels during atmospheric hydrogen sulfide exposure and intravenous sulfide infusion, FASEB J. 22 (2008) 749–750.
[19] H. Xu, M. Hepel, Molecular beacon"-based fluorescent assay for the selective detection of glutathione and cysteine, Anal. Chem. 83 (2011) 813–819.
[20] O. Rusin, N.N.S. Luce, R.A. Agbaria, J.O. Escobedo, S. Jiang, I.M. Warner, F.B. Dawan, K. Lian, R.M. Strongin, Visual detection of cysteine and homocysteine, J. Am. Chem. Soc. 126 (2004) 438–439.
[21] W. Wang, O. Rusin, X. Xu, K.K. Kim, J.O. Escobedo, S.O. Fakayode, K.A. Fletcher, M. Lowry, C.M. Schowalter, C.M. Lawrence, F.R. Fronczek, I.M. Warner, R.M. Strongin, Detection of homocysteine and cysteine, J. Am. Chem. Soc. 127 (2005) 15949–15958.
[22] F. Tanaka, N.C.F.B. Mase III, Determination of cysteine concentration by fluorescence increase: reaction of cysteine with a fluorogenic aldehyde, Chem. Commun. (2004) 1762–1763.
[23] W. Zhang, F. Wan, W. Zhu, H. Xu, X. Ye, R. Cheng, L.-T. Jin, Determination of glutathione and glutathione disulfide in hepatocytes by liquid chromatography with an electrode modified with functionalized carbon nanotubes, J. Chromatogr. B 818 (2005) 227–232.
[24] J. Vacek, B. Klejdus, J. Petrlova, L. Lojkova, V. Kuban, A hydrophilic interaction chromatography coupled to a mass spectrometry for the determination of glutathione in plant somatic embryos, Analyst 131 (2006) 1167–1174.
[25] C. Lu, Y. Zu, V.W.W. Yam, Nonionic surfactant-capped gold nanoparticles as postcolumn reagents for high-performance liquid chromatography assay of low-molecular-mass biothiols, J. Chromatogr. A 1163 (2007) 328–332.
[26] C.K. Chiang, Y.W. Lin, W.T. Chen, H.T. Chang, Accurate quantitation of glutathione in cell lysates through surface-assisted laser desorption/ionization mass spectrometry using gold nanoparticles, Nanomed. Nanotechnol. Biol. Med. 6 (2010) 530–537.
[27] N. Spătaru, B.V. Sarada, E. Popa, D.A. Tryk, A. Fujishima, Voltammetric determination of L-cysteine at conductive diamond electrodes, Anal. Chem. 73 (2001) 514–519.
[28] J.C. Ndamanisha, J. Bai, B. Qi, L. Guo, Application of electrochemical properties of ordered mesoporous carbon to the determination of glutathione and cysteine, Anal. Biochem. 386 (2009) 79–84.
[29] M. Stobiecka, J. Deeb, M. Hepel, Molecularly-templated polymer matrix films for biorecognition processes: sensors for evaluating oxidative stress and redox buffering capacity, Electrochem. Soc. Trans. 19 (2009) 15–32.
[30] E.J. Pacsial-Ong, R.L. McCarley, W. Wang, R.M. Strongin, Electrochemical detection of glutathione using redox indicators, Anal. Chem. 78 (2006) 7577–7581.
[31] F.X. Zhang, L. Han, L.B. Israel, J.G. Daras, M.M. Maye, N.K. Ly, C.J. Zhong, Colorimetric detection of thiol-containing amino acids using gold nanoparticles, Analyst 127 (2002) 462–465.
[32] P.K. Sudeep, S.T.S. Joseph, K.G. Thomas, Selective detection of cysteine and glutathione using gold nanorods, J. Am. Chem. Soc. 127 (2005) 6516–6517.
[33] H. Huang, X. Liu, T. Hu, P.K. Chu, Ultra-sensitive detection of cysteine by gold nanorod assembly, Biosens. Bioelectron. 25 (2010) 2078–2083.
[34] X. Kou, S. Zhang, Z. Yang, C.-K. Tsung, G.D. Stucky, L. Sun, J. Wang, C. Yan, Glutathione- and cysteine-induced transverse overgrowth on gold nanorods, J. Am. Chem. Soc. 129 (2007) 6402–6404.
[35] N. Uehara, K. Ookubo, T. Shimizu, Colorimetric assay of glutathione based on the spontaneous disassembly of aggregated gold nanocomposites conjugated with water-soluble polymer, Langmuir 26 (2010) 6818–6825.
[36] I.M.S. Lim, D. Mott, W. Ip, P.N. Njoki, Y. Pan, S. Zhou, C.J. Zhong, Interparticle interactions in glutathione mediated assembly of gold nanoparticles, Langmuir 24 (2008) 8857–8863.
[37] M. Stobiecka, M. Hepel, Rapid functionalization of metal nanoparticles by moderator-tunable ligand-exchange process for biosensor designs, Sens. Actuators B 149 (2010) 373–380.
[38] M. Stobiecka, J. Deeb, M. Hepel, Ligand exchange effects in gold nanoparticle assembly induced by oxidative stress biomarkers: homocysteine and cysteine, Biophys. Chem. 146 (2010) 98–107.
[39] M. Stobiecka, K. Coopersmith, M. Hepel, Resonance elastic light scattering (RELS) spectroscopy of fast non-langmuirian ligand-exchange in glutathione-induced gold nanoparticle assembly, J. Colloid Interface Sci. 350 (2010) 168–177.
[40] P. Skládal, Piezoelectric quartz crystal sensors applied for bioanalytical assays and characterization of affinity interactions, J. Braz. Chem. Soc. 14 (2003) 491–502.
[41] M. Pohanka, P. Skládal, Electrochemical biosensors—principles and applications, J. Appl. Biomed. 6 (2008) 57–64.
[42] A.E. Gerdon, D.W. Wright, D.E. Cliffel, Quartz crystal microbalance detection of glutathione-protected nanoclusters using antibody recognition, Anal. Chem. 77 (2005) 304–310.
[43] I.V. Safenkova, A.V. Zherdeva, B.B. Dzantiev, Correlation between the composition of multivalent antibody conjugates with colloidal gold nanoparticles and their affinity, J. Immunol. Methods 357 (2010) 17–25.
[44] M. Hepel, E. Tewksbury, Ion-gating phenomena of self-assembling glutathione films on gold piezoelectrodes, J. Electroanal. Chem. 552 (2003) 291–305.
[45] M. Hepel, E. Tewksbury, Nanogravimetric study of templated copper deposition in ion-channels of self-assembled glutathione films on gold piezoelectrodes, Electrochim. Acta 49 (2004) 3827–3840.
[46] R.M. Silverstein, G.C. Bassler, T.C. Morrill, Spectrometric Identification of Organic Compounds, John Wiley and Sons, New York, 1981.
[47] A. Rosei, Hydrogen bonding by the sulphydryl group of glutathione, Experientia 35 (1979) 1178–1179.
[48] A.E. Radkowsky, E.M. Kosower, D. Eisenberg, I. Goldberg, Bimanes 18. (Haloalkyl)-1,5-diazabicyclo[3.3.0]octadienediones (Halo-9,10-dioxabimanes): sulfur extraction by syn-(1-bromoethyl,methyl)bimane. Gluttathione sulphide from the tripeptide thiol glutathione, J. Am. Chem. Soc. 108 (1986) 4532–4541.
[49] D.R. Lide, CRC Handbook of Chemistry and Physics, CRC Press, Boca Raton, FL, 2003.